ACS APPLIED MATERIALS & INTERFACES

Research Article

www.acsami.org

# Novel Bis[5-(fluoren-2-yl)thiophen-2-yl]benzothiadiazole End-Capped with Carbazole Dendrons as Highly Efficient Solution-Processed Nondoped Red Emitters for Organic Light-Emitting Diodes

Narid Prachumrak,[†] Sirintra Pojanasopa,[†] Supawadee Namuangruk,[‡] Tinnagon Kaewin,[†] Siriporn Jungsuttiwong,[†] Taweesak Sudyoadsuk,[†] and Vinich Promarak*[,§]

[†]Department of Chemistry and Center for Innovation in Chemistry, Faculty of Science, Ubon Ratchathani University, Ubon Ratchathani, 34190 Thailand

[‡]National Nanotechnology Center (NANOTEC), 130 Thailand Science Park, Klong Luang, Pathumthani, 12120 Thailand

[§]School of Chemistry and Center for Innovation in Chemistry, Institute of Science, Suranaree University of Technology, Muang District, Nakhon Ratchasima, 30000 Thailand

Supporting Information

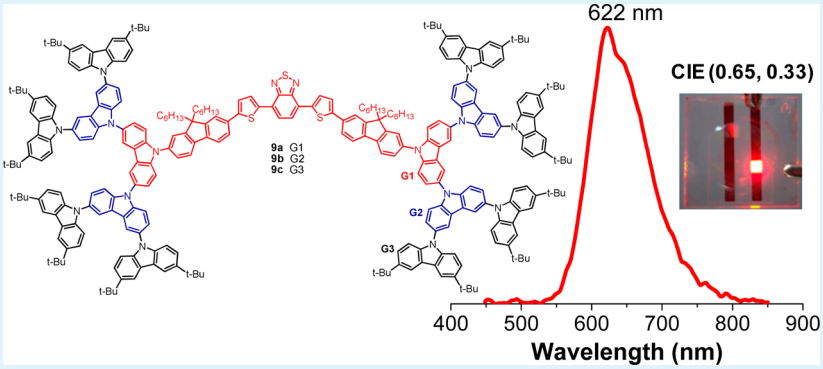


**ABSTRACT:** A series of novel red-emitting bis[5-(fluoren-2-yl)thiophen-2-yl]benzothiadiazole-cored dendrimers containing carbazole dendrons up to the third generation are synthesized. Their photophysical, thermal, electrochemical, and electroluminescent properties as nondoped solution-processed red light-emitters for OLEDs are investigated. By using carbazole dendrons as the end caps, we are able to reduce the crystallization and retain the high emissive ability of a planar fluorescent core in the solid state as well as improve the thermal stability of the material. These dendrimers show a bright-red fluorescence and can form morphologically stable amorphous thin films with glass-transition temperatures as high as 283 °C. Simple structured solution-processed OLEDs using these materials as hole-transporting nondoped emitters and BCP as the hole-blocking layer emit a stable red color around 622−645 nm, with high luminance efficiencies (up to 4.80 cd $A^{-1}$ at 1.2 mA $cm^{-2}$) and CIE coordinates of (0.65, 0.33), which are close to the pure red color.

**KEYWORDS:** *organic light-emitting diode, nondoped red emitter, dendrimer, carbazole dendron, benzothiadiazole, fluorene*

## INTRODUCTION

Since the first highly efficient multilayer organic light-emitting diodes (OLEDs) were reported by Tang and Van Slyke in 1987,[1] OLEDs have attracted great attention from the scientific community because of their potential applications in solid-state lighting and flat-panel displays.[2] OLEDs are characterized by their low driving voltage, high brightness, full-color emission, rapid response, and easy fabrication of potentially large-area, flexible thin-film devices. Current trends in the development of OLEDs are focusing mainly on the optimization of device structures and the development of new emitting materials. In terms of device fabrication, solution-processed OLEDs fabricated using molecular materials will have great advantages because the materials used are easy to synthesize and purify, and the fabrication method is convenient and low cost, allowing large-scale manufacturing with less material usage.[3] Research on novel luminescent materials has played a vital role in developing OLEDs. Both small molecules and polymers have been studied extensively for use in OLEDs.[4] Dendrimers are an alternative class of molecular electroluminescent (EL) materials.[5] Unlike polymers, the beauty of dendrimers is that their light emission can be finely tuned by the selection of the core, their solubility can be adjusted by selecting the proper surface groups, and their level of intermolecular interactions can be controlled by the type and generation of the dendrons employed, which are vital parts of the performance of

Received: June 17, 2013
Accepted: August 6, 2013
Published: August 21, 2013

   dx.doi.org/10.1021/am402349v | ACS Appl. Mater. Interfaces 2013, 5, 8694−8703

OLEDs.[5] To date, several types of fluorescent[6] and phosphorescent[7] light-emitting dendrimers have been reported that have been successfully used in the fabrication of OLEDs by means of a solution process.

Red OLEDs are a necessary component in full-color displays. To date, most of the reported molecular red emitters are dopants such as the 4-(dicyanomethylene)-2-methyl-6-[2-(2,3,6,7-tetrahydro-1*H*,5*H*-benzo[ij]quinolizin-9-yl)ethenyl]-4*H*-pyran (DCJ, DCM) series,[8] chromene-based and polyacene-based materials,[9] and rare-earth complexes.[10] Practically, OLEDs based on dopant emitters are more difficult to adapt for mass-production processes than those based on nondoped host emitters because of the reproducibility problems of reliably achieving the optimum doping concentration, which requires careful manufacturing control. Therefore, highly efficient nondoped red-fluorescent emitters for OLEDs are in great demand, but unfortunately there are only a few examples reported in the literature. The nondoped pure red emitters are especially very rare.[11−13] This is because fluorophores showing red emission either have extended $\pi$ conjugation or bear donor−acceptor polar substituents. Both types of red fluorophores are prone to crystallization in the solid state and hence are highly concentration quenching. Examples of nondoped red emitters reported in the literature are 1,10-dicyano-substituted bis-styrylnaphthalene derivative (BSN) ($\eta$ = 2.8 cd $A^{-1}$),[14] bis(4-(*N*-(1-naphthyl)phenylamino)phenyl)-fumaronitrile ($\eta$ = 2.5 cd $A^{-1}$ at 4 mA $cm^{-2}$),[15] binaphthyl-containing benzothiadiazole derivative ($\eta$ = 1.95 cd $A^{-1}$ at 59.2 mA $cm^{-2}$),[13] 1,4-bis(diarylamino)-2,5-bis(4-cyanophenylethenyl)benzenes ($\eta$ = 0.71 cd $A^{-1}$),[16] thieno-[3,4-*b*]-pyrazines-cored dendrimers ($\eta$ = 0.74 cd $A^{-1}$ at 16.5 mA $cm^{-2}$),[17,18] truxene-based gradient $\pi$-conjugated dendrimers ($\eta$ = 1.07 cd $A^{-1}$),[19] alkyl-linked peripheral carbazole-substituted dithienylbenzothiadiazole ($\eta$ = 0.22 cd $A^{-1}$),[20] dipolar pyrazine derivatives ($\eta$ = 1.07 cd $A^{-1}$ at 10.0 mA $cm^{-2}$),[21] nonplanar pentaphenylbenzene-functionalized benzo-[2,1,3]thiadiazole (1.37 cd $A^{-1}$),[22] 4,7-tetraphenylethene-functionalized di(thiophen-2-yl)benzo-2,1,3-thiadiazole ($\eta$ = 2.4 cd $A^{-1}$),[23] *N*-methyl-bis(4-(*N*-(1-naphthyl)-*N*-phenylamino)phenyl)maleimide (EQE = 1.6% at 14 mA $cm^{-2}$),[24] arylaminospirobifluorene-substituted fumaronitriles (EQE = 3.1% at 1 mA $cm^{-2}$),[25] and $\pi$-conjugated organoboron complexes ($\eta_{PE}$ = 0.53 lm $W^{-1}$).[26] Besides, most OLEDs of these materials are often fabricated using the hole-transporting layer and complexes. More recently, we reported the synthesis and properties of carbazole-triphenylamine end-capped di-(thiophen-2-yl)benzothiadiazole, which proves to be an efficient solution-processed nondoped red emitter for a pure red OLED.[27] A simple double-layer OLED based on this material emits stable pure red light at 653 nm (CIE = 0.66, 0.33), with a luminance efficiency as high as 3.97 cd $A^{-1}$ at 3.2 mA $cm^{-2}$. However, new classes of solution-processed nondoped red emitters with improvements in terms of material property, device efficiency, and color purity remain to be explored. To this end, we prepared and investigated new solution-processed dendrimer-based red emitters (Scheme 1). Our design involves the use of bis[5-(fluoren-2-yl)thiophen-2-yl]benzothiadiazole as a fluorescent core and carbazole dendrimers up to the third generation as end-capping groups. The latter can suppress the aggregation-induced fluorescence quenching of the planar conjugated core as well as increase the hole-transporting capability, thermal stability, and solubility of the molecule. With the push−pull character of a combined end-capping group and core, the molecule will emit in the red region. Recently, we also reported on carbazole dendrimers that are successfully used as efficient solution-processed high-$T_g$ amorphous hole-transporting materials for Alq3-based green OLEDs.[28] With this design, a simple solution-processed hole-transporting nondoped red emitter can be obtained, and a simple structure nondoped red OLED can be fabricated. Herein, we report a detailed synthesis of a series of bis[5-(fluoren-2-yl)thiophen-2-yl]benzothiadiazole end-capped with carbazole dendrons (Scheme 1) as well as their physical and photophysical properties. The investigation of the solution-processed red OLED device fabrication and performance is also reported.

## EXPERIENTAL SECTION

**Materials and Methods.** All reagents were purchased from Aldrich, Acros, or Fluka and were used without further purification. All solvents were supplied by Thai companies and used without further distillation. Tetrahydrofuran (THF) was refluxed with sodium and benzophenone and distilled. $CH_2Cl_2$ for cyclic voltammetry (CV) measurements was washed with concd $H_2SO_4$ and distilled twice from calcium hydride. Chromatographic separations were carried out on silica gel (Merck silica gel 60) (0.0630−0.200 mm). $^1H$ and $^{13}C$ nuclear magnetic resonance (NMR) spectra were recorded on a Brüker AVANCE 300 MHz spectrometer with tetramethylsilane as the internal reference using $CDCl_3$ as the solvent in all cases. Ultraviolet−visible (UV−vis) spectra were recorded as a $CH_2Cl_2$ solution on a PerkinElmer UV Lambda 25 spectrometer. Photoluminescence spectra and the fluorescence quantum yields ($\Phi_F$) were recorded with a PerkinElmer LS 50B luminescence spectrometer as a $CH_2Cl_2$ solution, and thin films were obtained by spin casting. The fluorescence quantum yields ($\Phi_F$) were determined by a comparison with the fluorescence standard, coumarin 6 in ethanol ($\Phi_F$ = 0.78).[29] Differential scanning calorimetry (DSC) analysis and thermogravimetry analysis (TGA) were performed on a Mettler DSC823e thermal analyzer and a Rigaku TG-DTA 8120 thermal analyzer, respectively, with a heating rate of 10 °C $min^{-1}$ under a nitrogen atmosphere. Cyclic voltammetry (CV) measurements were carried out on an Autolab potentiostat PGSTAT 12 with a three-electrode system (platinum counter electrode, glassy carbon working electrode, and Ag/$Ag^+$ reference electrode) at a scan rate of 50 mV $s^{-1}$ in $CH_2Cl_2$ under an argon atmosphere. The concentration of analytical materials and tetrabutyl ammonium hexafluorophosphate (*n*-$Bu_4NPF_6$) were $10^{-3}$ and 0.1 M, respectively. Melting points were measured using an Electrothermal IA 9100 series digital melting-point instrument and are uncorrected. MALDI-TOF mass spectra were recorded on Bruker Daltonics (Bremen, Germany) Autoflex II matrix-assisted laser desorption/ionization-time of flight mass spectrometer (BIFEX) using $\alpha$-cyano-4-hydroxycinnamic acid as a matrix. The atomic force microscopy (AFM) analysis was performed on Park System model XE 100 using a standard noncontact mode with a resonance of 316.17 kHz.

**Synthesis of Compounds.** *7-Bromo-2-(thiophene-2-yl)-9,9-dihexylfluorene (**2**).* A mixture of **1**[30] (1.1 g, 2.23 mmol), 2-thiopheneboronic acid (0.35 g, 2.73 mmol), $Pd(PPh_3)_4$ (0.08 g, 0.07 mmol), and a 2 M $Na_2CO_3$ aqueous solution (7 mL) in THF (70 mL) was degassed with $N_2$ for 5 min. The reaction mixture was stirred at reflux under $N_2$ for 24 h. After the mixture was cooled to room temperature, water (70 mL) was added, and the mixture was extracted with $CH_2Cl_2$ (70 mL × 3). The combined organic phases were washed with water (100 mL) and brine solution (100 mL), dried over anhydrous $Na_2SO_4$, and filtered, and the solvents were removed to dryness. Purification by column chromatography over silica gel and eluting with a mixture of $CH_2Cl_2$ and hexane (2:3) followed by recrystallization with a mixture of $CH_2Cl_2$ and methanol gave the product as a white solid (1.17 g, 87%). $^1H$ NMR (300 MHz, $CDCl_3$) $\delta$ 0.63−0.66 (m, 6H), 0.75−0.79 (m, 4H), 1.06−1.15 (m, 12H), 1.56−2.00 (m, 4H), 7.11 (dd, *J* = 3.6 Hz, *J* = 1.5 Hz, 1H), 7.29 (d, *J* = 8.1


dx.doi.org/10.1021/am402349v | ACS Appl. Mater. Interfaces 2013, 5, 8694−8703

Hz, 1H), 7.37 (d, $J$ = 3.6 Hz, 1H), 7.44−7.46 (m, 2H), 7.53−7.56 (m, 2H), 7.61 (dd, $J$ = 11.1 Hz, $J$ = 1.2 Hz, 1H), 7.64 (d, $J$ = 7.8 Hz) ppm; $^{13}$C NMR (75 MHz, $CDCl_3$) $\delta$ 13.94, 22.53, 23.67, 29.59, 31.43, 40.29, 55.50, 119.99, 120.18, 123.02, 124.66, 125.07, 126.16, 128.05, 130.01, 133.67, 139.56, 139.67, 144.97, 151.61, 153.13 ppm; MALDI-TOF ($m/z$) ($M^+$) calcd for $C_{29}H_{35}BrS$: 494.164; found, 494.161.

*2-[7-(3,6-Ditert-butylcarbazol-N-yl)fluoren-2-yl]thiophene (**3**).* A mixture of **2** (1.20 g, 2.43 mmol), 3,6-di-*tert*-butylcarbazole (**G1-H**)[28] (0.80 g, 2.86 mmol), CuI (0.67 g, 3.5 mmol), $K_3PO_4$ (3.71 g, 17.50 mmol), and ±*trans*-1,2-diaminocyclohexane (0.40 g, 3.5 mmol) in toluene (60 mL) was stirred at 110 °C under a $N_2$ atmosphere for 24 h. After cooling, the reaction mixture was extracted with $CH_2Cl_2$ (70 mL × 3). The combined organic phases were washed with water (100 mL) and brine solution (100 mL), dried over anhydrous $Na_2SO_4$, and filtered, and the solvents were removed to dryness. The crude product was purified by column chromatography on silica gel and eluted with a mixture of $CH_2Cl_2$ and hexane (1:3) to give the product as a white solid (1.21 g, 76%). $^1$H NMR (300 MHz, $CDCl_3$) $\delta$ 0.79−0.84 (m, 10H), 1.13−1.21 (m, 12H), 1.50 (s, 18H), 2.02−2.07 (m, 4H), 7.16 (t, $J$ = 4.2 Hz, 1H), 7.33 (d, $J$ = 5.1 Hz), 7.41−7.44 (m, 3H), 7.49−7.57 (m, 4H), 7.63 (d, $J$ = 1.5 Hz, 1H), 7.66 (d, $J$ = 8.2 Hz, 1H), 7.76 (d, $J$ = 8.7 Hz, 1H), 7.89 (d, $J$ = 8.5 Hz, 1H), 8.19 (d, $J$ = 1.8 Hz, 2H) ppm; $^{13}$C NMR (75 MHz, $CDCl_3$) $\delta$ 14.06, 22.60, 23.91, 29.69, 31.56, 32.06, 34.77, 40.38, 55.49, 109.25, 116.33, 120.20, 120.24, 120.74, 121.41, 123.01, 123.39, 123.58, 124.65, 125.14, 125.41, 128.11, 133.45, 136.95, 139.37, 139.46, 140.00, 142.82, 145.09, 151.82, 152.64 ppm; MALDI-TOF ($m/z$) ($M^+$) calcd for $C_{49}H_{59}NS$: 693.437; found, 693.442.

*2-{7-[3,6-Bis(3,6-ditert-butylcarbazol-N-yl)carbazole-N-yl]-fluoren-2-yl}thiophene (**4**).* Compound **4** was synthesized from **2** and **G2-H**[28] in similar manner to that of **3** and was obtained as a white solid (77%). mp >200 °C; $^1$H NMR (300 MHz, $CDCl_3$) $\delta$ 0.76−0.87 (m, 10H), 1.14−1.27 (m, 12H), 1.48 (s, 36H), 2.10−2.15 (m, 4H), 7.15−7.17 (m, 1H), 7.34−7.38 (m, 5H), 7.44−7.49 (m, 5H), 7.65−7.72 (m, 8H), 7.81 (d, $J$ = 8.1 Hz, 1H), 7.99 (d, $J$ = 8.4 Hz, 1H), 8.18 (s, 4H), 8.28 (s, 2H) ppm; $^{13}$C NMR (75 MHz, $CDCl_3$) $\delta$ 14.02, 22.53, 23.97, 29.65, 31.53, 32.06, 34.75, 40.37, 55.68, 109.12, 111.12, 116.23, 119.40, 120.34, 120.46, 121.11, 121.81, 123.16, 123.58, 123.97, 124.81, 125.93, 126.00, 128.14, 130.88, 133.89, 135.88, 139.64, 140.21, 140.61, 140.63, 142.58, 144.93, 151.88, 153.14 ppm; MALDI-TOF ($m/z$) ($MH^+$) calcd for $C_{81}H_{90}N_3S$: 1136.686; found, 1136.678.

*2-{7-{3,6-Bis[3,6-bis(3,6-ditert-butylcarbazol-N-yl)carbazole-N-yl]carbazole-N-yl}fluoren-2-yl}thiophene (**5**).* Compound **5** was synthesized from **2** and **G3-H**[28] in similar manner to that of **3** and was obtained as a white solid (73%). mp >200 °C; $^1$H NMR (300 MHz, $CDCl_3$) $\delta$ 0.81−0.91 (m, 10H), 1.20−1.28 (m, 12H), 1.49 (s, 72H), 2.16−2.21 (m, 4H), 7.18−7.19 (m, 1H), 7.32−7.40 (m, 10H), 7.47−7.51 (m, 10H), 7.64−7.90 (m, 14H), 8.07 (d, $J$ = 9.3 Hz, 2H), 8.19 (d, $J$ = 1.3 Hz, 8H), 8.31 (d, $J$ = 1.0 Hz, 4H), 8.60 (s, 2H) ppm; $^{13}$C NMR (75 MHz, $CDCl_3$) $\delta$ 14.05, 22.55, 24.03, 29.66, 31.55, 31.79, 31.88, 31.98, 34.63, 34.73, 40.35, 55.77, 103.47, 104.18, 108.76, 109.91, 110.23, 111.41, 115.28, 115.52, 115.84, 120.04, 120.65, 121.35, 121.93, 122.15, 122.37, 122.58, 123.31, 124.21, 125.41, 126.14, 126.33, 128.24, 128.64, 130.08, 130.58, 130.78, 130.95, 133.20, 136.67, 136.80, 137.58, 141.07, 141.18, 142.12, 124.58, 143.18, 143.88, 144.52, 146.50, 152.05, 153.31 ppm; MALDI-TOF ($m/z$) ($MH^+$) calcd for $C_{145}H_{150}N_7S$: 2021.167; found, 2021.159.

*5-Bromo-2-[7-(3,6-ditert-butylcarbazol-N-yl)fluoren-2-yl]-thiophene (**6**).* To a solution of **3** (0.1 g, 0.24 mmol) in THF (20 mL) was added with *N*-bromosuccinimide (0.05 g, 0.27 mmol) in small portions. The reaction mixture was stirred at room temperature for 20 min. Water (50 mL) was added, and the mixture was extracted with $CH_2Cl_2$ (50 mL × 3). The combined organic phases were washed with water (70 mL) and brine solution (70 mL), dried over anhydrous $Na_2SO_4$, and filtered, and the solvents were removed to dryness. Purification by column chromatography over silica gel and eluting with a mixture of $CH_2Cl_2$ and hexane (1:3) followed by recrystallization with a mixture of $CH_2Cl_2$ and methanol gave the product as a light-yellow solid (0.16 g, 90%). $^1$H NMR (300 MHz, $CDCl_3$) $\delta$ 0.78−0.83 (m, 10H), 1.12−1.18 (m, 12H), 1.50 (s, 18 H), 1.99−2.05 (m, 4H), 7.08 (d, $J$ = 3.6 Hz, 1H), 7.16 (d, $J$ = 3.6 Hz, 1H), 7.39 (d, $J$ = 8.4 Hz, 2H), 7.48−7.58 (m, 4H), 7.47 (d, $J$ = 7.8 Hz, 1H), 7.88 (d, $J$ = 8.4 Hz, 1H), 8.18 (d, $J$ = 1.8 Hz, 2H) ppm; $^{13}$C NMR (75 MHz, $CDCl_3$) $\delta$ 14.13, 22.58, 23.88, 29.64, 31.53, 32.76, 34.76, 40.32, 55.49, 109.21, 111.13, 116.32, 119.88, 120.30, 120.83, 121.38, 123.10, 123.38, 123.57, 124.79, 125.42, 130.89, 132.62, 137.12, 139.20, 139.30, 140.40, 142.85, 146.52, 151.94, 152.63 ppm; MALDI-TOF ($m/z$) ($M^+$) calcd for $C_{49}H_{58}BrNS$: 771.347; found, 771.335.

*5-Bromo-2-{7-[3,6-bis(3,6-ditert-butylcarbazol-N-yl)carbazole-N-yl]fluoren-2-yl}thiophene (**7**).* Compound **7** was synthesized from **4** in similar manner to that of **6** and was obtained as a light-yellow solid (84%). mp >200 °C; $^1$H NMR (300 MHz, $CDCl_3$) $\delta$ 0.75−0.86 (m, 10H), 1.13−1.26 (m, 12H), 1.47 (s, 36H), 2.08−2.13 (m, 4H), 7.08 (d, $J$ = 3.9 Hz, 1H), 7.17 (d, $J$ = 3.6 Hz, 1H), 7.14 (d, $J$ = 8.7 Hz, 4H), 7.45 (dd, $J$ = 8.7 Hz, $J$ = 1.2 Hz, 4H), 7.55−7.72 (m, 8H), 7.80 (d, $J$ = 7.8 Hz, 1H), 7.99 (d, $J$ = 8.4 Hz, 1H), 8.12−8.26 (m, 6 H) ppm; $^{13}$C NMR (75 MHz, $CDCl_3$) $\delta$ 14.04, 22.55, 24.00, 29.68, 31.55, 31.90, 32.06, 34.74, 40.41, 55.71, 109.11, 111.12, 116.23, 119.41, 119.96, 120.56, 121.16, 121.81, 123.15, 123.58, 123.98, 124.61, 124.91, 126.00, 130.89, 133.47, 135.97, 136.73, 139.86, 140.20, 140.54, 140.58, 142.58, 143.69, 151.99, 153.15 ppm; MALDI-TOF ($m/z$) ($MH^+$) calcd for $C_{81}H_{89}BrN_3S$: 1214.596; found, 1214.589.

*5-Bromo-2-{7-{3,6-bis[3,6-bis(3,6-ditert-butylcarbazol-N-yl)-carbazole-N-yl]carbazole-N-yl}fluoren-2-yl}thiophene (**8**).* Compound **8** was synthesized from **5** in similar manner to that of **6** and was obtained as a light-yellow solid (85%). mp >200 °C; $^1$H NMR (300 MHz, $CDCl_3$) $\delta$ 0.82−0.92 (m, 10H), 1.20−1.29 (m, 12H), 1.50 (s, 72H), 2.17−2.20 (m, 4H), 7.11 (d, $J$ = 3.6 Hz, 1H), 7.20 (d, $J$ = 3.6 Hz, 1H), 7.41 (d, $J$ = 8.7 Hz, 8H), 7.49 (dd, $J$ = 8.6 Hz, 8H), 7.61−7.72 (m, 10H), 7.81−7.90 (m, 6H), 8.07 (d, $J$ = 8.4 Hz, 1H), 8.15−8.21 (m, 9H), 8.32 (s, 4H), 8.61 (s, 2H) ppm; $^{13}$C NMR (75 MHz, $CDCl_3$) $\delta$ 14.04, 22.54, 24.02, 29.64, 31.54, 31.89, 32.05, 34.73, 40.35, 55.79, 109.12, 111.07, 111.49, 111.72, 116.20, 119.43, 120.10, 120.69, 121.39, 121.94, 123.14, 123.36, 123.55, 123.82, 124.15, 124.33, 125.03, 126.04, 126.45, 130.04, 130.81, 130.97, 133.29, 135.69, 139.91, 140.25, 140.89, 141.36, 141.44, 142.56, 146.29, 152.03, 153.37 ppm; MALDI-TOF ($m/z$) ($MH^+$) calcd for $C_{145}H_{149}BrN_7S$: 2099.078; found, 2099.077.

*4,7-Bis{5-[7-(3,6-ditert-butylcarbazol-N-yl)fluoren-2-yl]thiophen-2-yl}benzothiadiazole (**9a**).* A mixture of **6** (0.50 g, 0.41 mmol), 2,1,3-benzothiadiazole-4,7-bis(boronic acid pinacol ester) (0.04 g, 0.10 mmol), $Pd(PPh_3)_4$ (0.003 g, 0.003 mmol), and a 2 M $Na_2CO_3$ aqueous solution (3 mL) in THF (30 mL) was degassed with $N_2$ for 5 min. The reaction mixture was stirred at reflux under $N_2$ for 24 h. After the mixture was cooled to room temperature, water (70 mL) was added, and the mixture was extracted with $CH_2Cl_2$ (70 mL × 3). The combined organic phases were washed with water (70 mL) and brine solution (70 mL), dried over anhydrous $Na_2SO_4$, and filtered, and the solvents were removed to dryness. Purification by column chromatography over silica gel and eluting with a mixture of $CH_2Cl_2$ and hexane (1:9) followed by recrystallization with a mixture of $CH_2Cl_2$ and methanol gave the product as a red solid (0.11 g, 76%). mp >200 °C; $^1$H NMR (300 MHz, $CDCl_3$) $\delta$ 0.79−0.95 (m, 20H), 1.14−1.26 (m, 24H), 1.49 (s, 36H), 2.06−2.08 (m, 8H), 7.43 (d, $J$ = 9.6 Hz, 4H), 7.48−7.56 (m, 10H), 7.72−7.79 (m, 6 H), 7.89 (d, $J$ = 8.4 Hz), 7.97 (s, 2H), 8.18 (s, 6H) ppm; $^{13}$C NMR (75 MHz, $CDCl_3$) $\delta$ 14.04, 22.60, 23.94, 29.71, 31.57, 32.04, 34.76, 40.40, 55.56, 109.24, 116.32, 120.12, 120.29, 120.81, 121.42, 123,41, 124.08, 123.57, 125.04, 125.36, 125.44, 125.86, 128.71, 133.16, 137.09, 138.50, 139.35, 140.43, 146.85, 151.93, 152.71 ppm; FT-IR (KBr) $\nu$ 2958, 2933, 2852, 1631, 1611, 1580, 1484, 1467, 1452, 1362, 1334, 1294, 1262, 1233, 1100, 1031, 877, 808 $cm^{-1}$; MALDI-TOF ($m/z$) ($M^+$) calcd for $C_{101}H_{110}N_4S_3$: 1474.789; found, 1474.779.

*4,7-Bis{5-{7-[3,6-bis(3,6-ditert-butylcarbazol-N-yl)carbazole-N-yl]fluoren-2-yl}thiophene-2-yl}benzothiadiazole (**9b**).* Compound **9b** was synthesized from **7** in similar manner to that of **9a** and was obtained as a red solid (65%). mp >200 °C; $^1$H NMR (300 MHz, $CDCl_3$) $\delta$ 0.77−0.88 (m, 20H), 1.16−1.27 (m, 24H), 1.48 (s, 72H), 2.10−2.20 (m, 8H), 7.29 (d, $J$ = 3.6 Hz, 2H), 7.35−7.41 (m, 10H), 7.47 (dd, $J$ = 8.7 Hz, $J$ = 1.5 Hz, 8H), 7.62−7.73 (m, 16H), 7.83 (d, $J$ =

**Scheme 1. Synthesis of Red-Light Emitting Dendrimers 9a−c**

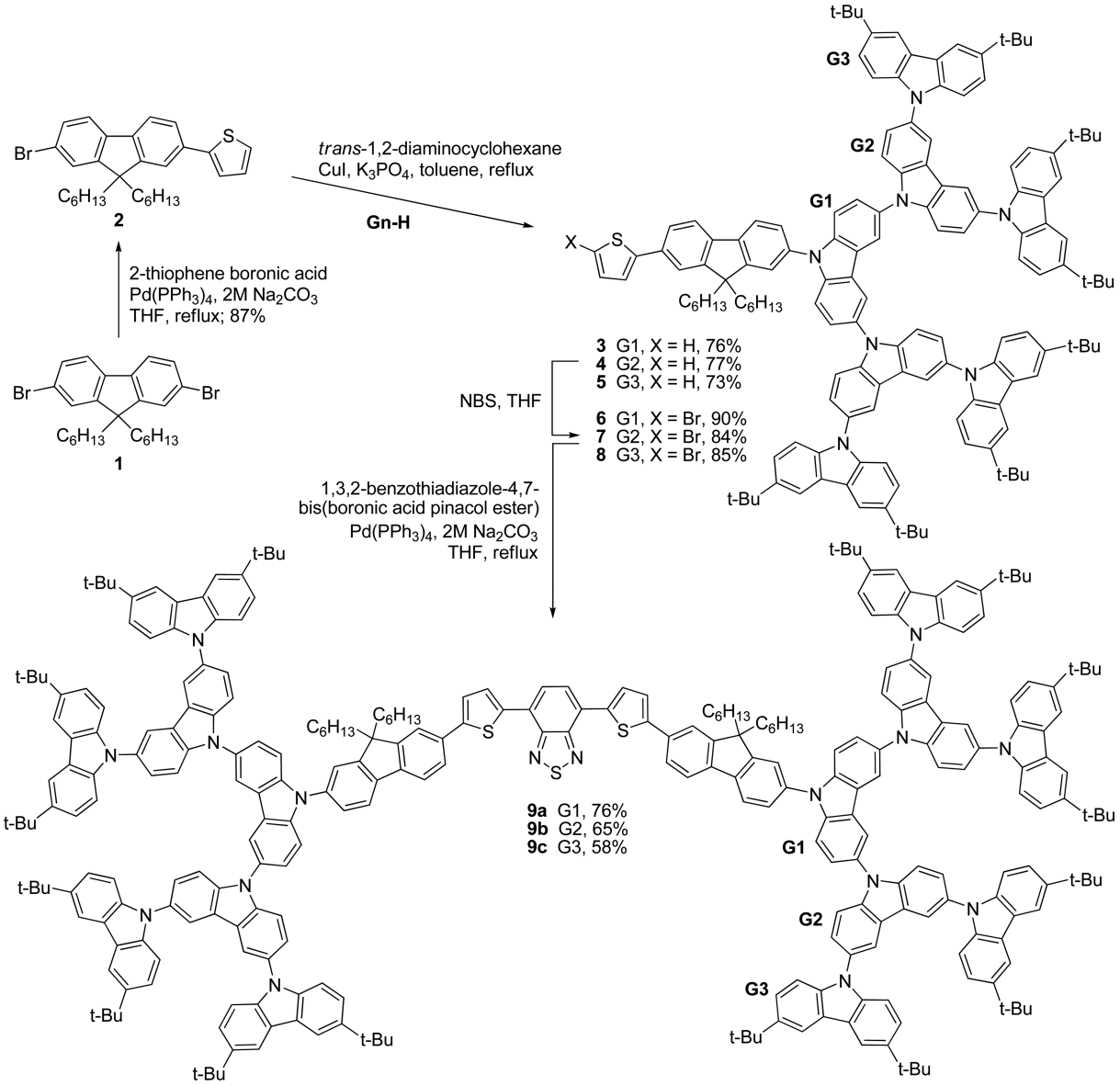


7.9 Hz, 2H), 8.01 (d, $J$ = 8.4 Hz, 2H), 8.13−8.18 (m, 10H), 8.28 (s, 4H) ppm; $^{13}$C NMR (75 MHz, $CDCl_3$) $\delta$ 14.06, 22.56, 22.70, 24.03, 29.69, 31.56, 31.91, 32.01, 32.07, 34.75, 38.77, 40.42, 55.77, 109.12, 111.13, 116.24, 119.42, 120.21, 120.57, 120.57, 121.22, 121.83, 123.11, 123.16, 123.59, 124.00, 124.25, 125.19, 125.41, 125.88, 126.01, 128.74, 130.90, 133.60, 136.02, 138.66, 140.09, 140.21, 140.31, 140.32, 140.59, 142.50, 142.59, 146.23, 152.01, 152.69, 153.21 ppm; FT-IR (KBr) $\nu$ 2953, 2923, 2854, 1659, 1640, 1631, 1609, 1491, 1483, 1467, 1449, 1362, 1322, 1296, 1261, 1232, 1022, 877, 807 cm$^{-1}$; MALDI-TOF ($m/z$) ($MH^+$) calcd for $C_{168}H_{179}N_8S_3$: 2404.341; found, 2404.340.

*4,7-Bis{5-{7-{3,6-bis[3,6-bis(3,6-ditert-butylcarbazol-N-yl)-carbazole-N-yl]carbazole-N-yl}fluoren-2-yl}thiophene-2-yl}-benzothiadiazole (**9c**).* Compound **9c** was synthesized from **8** in similar manner to that of **9a** and was obtained as a red solid (58%). mp >200 °C; $^1$H NMR (300 MHz, $CDCl_3$) $\delta$ 0.81−0.92 (m, 20H), 1.21−1.27 (m, 24H), 1.48 (s, 144H), 2.19−2.22 (m, 8H), 7.36 (d, $J$ = 8.4 Hz, 16H), 7.47 (dd, $J$ = 8.7 Hz, $J$ = 1.5 Hz, 16H), 7.59−7.71 (m, 18H), 7.82−7.93 (m, 18H), 8.01 (s, 2H), 8.01−8.23 (m, 20H), 8.30 (s, 8H), 8.60 (s, 4H) ppm; $^{13}$C NMR (75 MHz, $CDCl_3$) $\delta$ 14.12, 22.60, 24.07, 29.38, 29.72, 31.61, 31.91, 32.07, 34.75, 40.45, 55.86, 109.13, 111.10, 111.76, 116.23, 119.45, 120.14, 120.25, 1210.70, 121.40, 121.94, 123.13, 123.58, 123.82, 124.15, 124.34, 125.27, 125.90, 126.06, 126.47, 128.77, 130.02, 130.79, 133.80, 134.64, 138.75, 139.95, 140.23, 141.03, 141.36, 141.43, 142.56, 146.17, 152.02, 152.71, 153.42 ppm; FT-IR (KBr) $\nu$ 2958, 2861, 1629, 1608, 1587, 1474, 1452, 1322, 1294, 1278, 1259, 1241, 1030, 1022, 875, 807 cm$^{-1}$; MALDI-TOF ($m/z$) ($MH^+$) calcd for $C_{296}H_{299}N_{16}S_3$: 4173.305; found, 4173.332.

**Quantum Chemical Calculation.** The ground-state geometries of **9a−c** were fully optimized using density functional theory (DFT) at the B3LYP/6-31G (d,p) level, as implemented in Gaussian 09.[31] TDDFT/B3LYP calculations of the lowest excitation energies were performed at the optimized geometries of the ground states.

**Device Fabrication and Testing.** All red OLED devices using **9a−c** as nondoped missive layers (EML) with the device configurations of ITO/**9c** (spin-coating)/LiF(0.5 nm)−Al(150 nm), ITO/PEDOT−PSS/**9c** (spin-coating)/LiF(0.5 nm)−Al(150 nm), and ITO/PEDOT−PSS/**9a−c** (spin-coating)/BCP(40 nm)/LiF(0.5 nm)/Al(150 nm) were fabricated and characterized as follows. The patterned indium tin oxide (ITO) glass substrate with a sheet resistance of 14 ohm sq$^{-1}$ (purchased from Kintec Company) was thoroughly cleaned by successive ultrasonic treatments with detergent, deionized water, isopropanol, and acetone and dried at 60 °C in a vacuum oven. A 50 nm thick PEDOT/PSS hole injection layer was spin coated on top of the ITO from a 0.75 wt % dispersion in water at a spin speed of 3000 rpm for 20 s followed by drying at 200 °C for 15

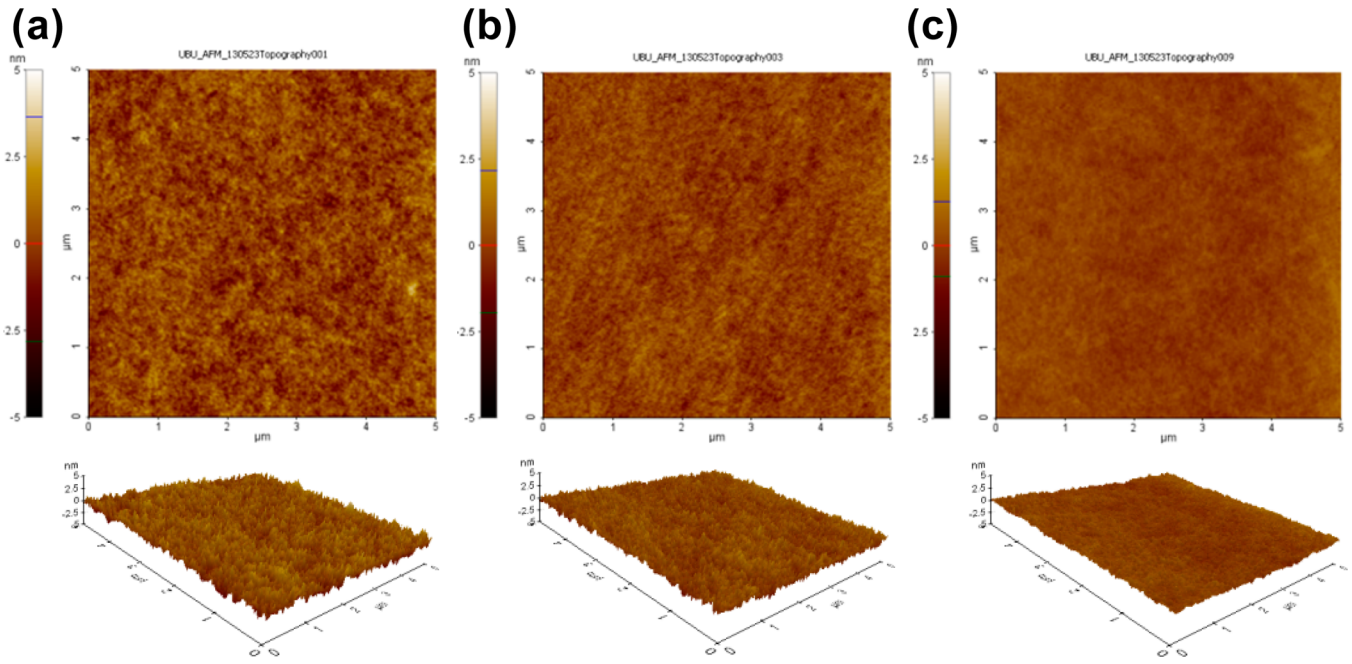


**Figure 1.** Tapping-mode AFM images of the spin-coated films of **9a–c**.

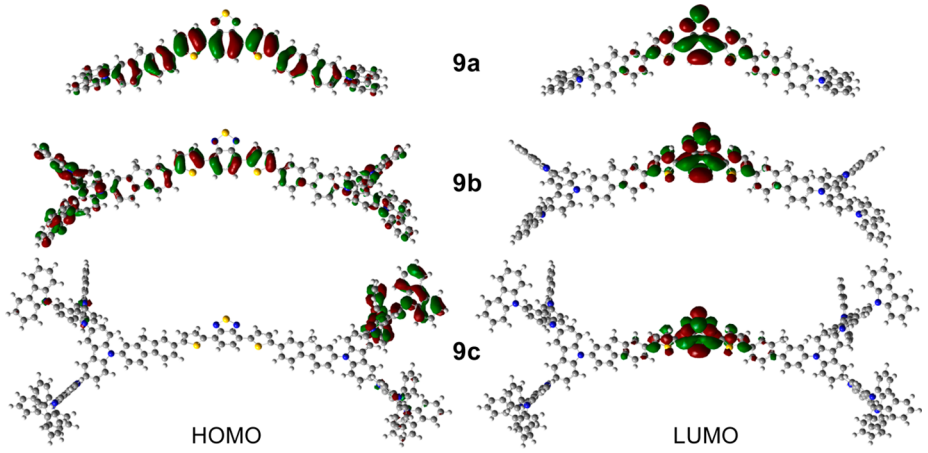


**Figure 2.** HOMO and LUMO of **9a–c** calculated by the TDDFT/B3LYP/6-31G (d,p) method.

min under vacuum. Thin films of **9a–c** were deposited on top of the ITO or PEDOT/PSS layers by spin coating a $CHCl_3$/toluene solution (1:1) of **9a–c** (1.5% w/v) at a spin speed of 3000 rpm for 30 s to get a 30–40 nm thick EML. The film thickness was measured using a Tencor $\alpha$-Step 500 surface profiler. The BCP layer was deposited onto the surface of the EML film as an electron-transporting layer (ETL) with a thickness of 40 nm by evaporation from resistively heated alumina crucibles at an evaporation rate of 0.5–1.0 nm $s^{-1}$ in a vacuum evaporator depositor (ES280, ANS Technology) under a base pressure of $\sim 10^{-5}$ mbar. The film thickness was monitored and recorded by a quartz oscillator thickness meter (TM-350, MAXTEK). The chamber was vented with dry air to load the cathode materials and pumped back; 0.5 nm thick lithium fluoride (LiF) and a 150 nm thick aluminum (Al) layers were subsequently deposited through a shadow mask on the top of the BCP film without braking the vacuum to form an active diode area of 4 $mm^2$. The measurement of the device efficiency was performed according to M.E. Thomson's protocol, and the external quantum efficiencies of the device were calculated using a procedure reported previously.[32] Current density–voltage–luminescence ($J$–$V$–$L$) characteristics were measured simultaneously with the use of a Keithley 2400 source meter and a Newport 1835C power meter equipped with a Newport 818-UV/CM calibrated silicon photodiode. The electroluminescent spectra were recorded with an Ocean Optics USB4000 multichannel spectrometer. All of the measurements were performed under an ambient atmosphere at room temperature shortly after breaking the chamber.

## RESULTS AND DISCUSSION

**Synthesis and Characterization.** Target carbazole dendrimers **9a–c** were synthesized by means of double palladium-catalyzed cross-coupling reactions of bromide intermediates **6–8**, as outlined in Scheme 1. In this synthesis, first 2,7-dibromofluorene **1**[30] was coupled with 2-thiophene boronic acid under Suzuki cross-coupling conditions catalyzed by $Pd(PPh_3)_4/Na_2CO_3$ in THF to give compound **2** in a good yield. Ullmann coupling of **2** (1.5 equiv) with available carbazole dendrons (**Gn-H**)[28] catalyzed by $CuI/K_3PO_4$/±*trans*-1,2-diaminocyclohexane in toluene provided corresponding thiophenes **3–5** in 73–76% yields. The bromination of compounds **3–5** with NBS in THF yielded bromides **6–8** in good yields. Double cross-coupling of **6–8** with 2,1,3-benzothiadiazole-4,7-bis(boronic acid pinacol ester) under

**Table 1. Photophysical, Physical, and Electrochemical Data for Dendrimers 9a–c**

| compound | $\lambda_{abs}^{solu}$ (nm)[a] | $\lambda_{em}^{solu}/\lambda_{em}^{sol}$ (nm)[b] | Stokes shift (nm)[c] | $\Phi_F$ (%)[d] | $T_g/T_{5d}$ (°C)[e] | $E_{1/2}$ vs $Ag/Ag^+$ (V)[f] | $E_g^{opt}/E_g^{ele}$ (eV)[g] | HOMO/LUMO (eV)[h] |
|---|---|---|---|---|---|---|---|---|
| **9a** | 298, 370, 513 | 611/630 | 98 | 0.39 | 115/326 | −1.69, −1.22, 0.94, 1.10, 1.22, 1.41 | 2.08/2.05 | −5.33/−3.25 |
| **9b** | 298, 371, 514 | 608/625 | 94 | 0.15 | 256/344 | −1.69, −1.20, 1.04, 1.19 | 2.07/2.07 | −5.38/−3.31 |
| **9c** | 298, 372, 514 | 606/616 | 92 | 0.10 | 283/378 | −1.69, −1.15, 1.02, 1.17 | 2.08/2.09 | −5.40/−3.32 |

[a]Measured in $CH_2Cl_2$. [b]Measured in $CH_2Cl_2$ and as thin films. [c]Calculated from the difference of $\lambda_{abs}^{solu}$ and $\lambda_{em}^{solu}$. [d]Measured in $CH_2Cl_2$ using coumarin 6 as a standard. [e]Obtained from DSC/TGA measured at a rate of 10 °C $min^{-1}$ under $N_2$. [f]Obtained from CV measured at a scan rate of 50 mV $s^{-1}$ in $CH_2Cl_2$ and $n$-$Bu_4NPF_6$ as the electrolyte. [g]Calculated from $E_g^{opt} = 1240/\lambda_{onset}$; $E_g^{ele} = E^{re}_{onset} - E^{ox}_{onset}$. [h]Estimated from HOMO = $-(4.44 + E^{ox}_{onset})$; LUMO = $E_g^{opt}$ − HOMO.

Suzuki-coupling conditions afforded desired bis[5-(fluoren-2-yl)thiophen-2-yl]benzothiadiazole-cored carbazole dendrimers **9a–c** as red solids in moderate to good yields of 58–76%. All newly synthesized compounds, **9a–c**, were fully characterized with $^1H$ NMR, $^{13}C$ NMR, FT-IR, and MALDI-TOF MS and were found to be in good agreement with the structures. These dendrimers exhibit a high solubility in most organic solvents, allowing their thin films to be fabricated by a solution-casting process, which overcomes the high cost of the vacuum-deposition process. The morphology of their spin-casting films, which is another key factor for OLEDs fabrication, was investigated by atomic force microscopy (AFM). The AFM image (Figure 1c) of the film spin coated from a $CHCl_3$/toluene solution of **9c** shows a very uniform and flat surface, indicating excellent film-forming properties. The surface of the spin-coated film of **9b** is rougher, whereas the thin film of **9a**, having the first generation of carbazole dendron as the end caps, shows the roughest surface among this series (Figure 1a,b). These AFM images give evidence that the film uniformity is mostly determined by the generation or size of the dendrimers and that in high-generation films the dendrimer branches can relatively easily interpenetrate each other and establish intermolecular interactions. This stable homogeneous amorphous morphology appears favorable for producing OLEDs with reduced leak currents and improved thermal stability during device operation.[33]

**Quantum Chemical Calculations.** To understand the geometries and the electronic properties of the dendrimers, quantum chemical calculations were performed using the TDDFT/B3LYP/6-31G (d,p) method.[31] Their optimized structures reveal increasingly sterically hindered structures of the dendrons surrounding the planar bis[5-(fluoren-2-yl)-thiophen-2-yl]benzothiadiazole core as the generation of the dendron increased (Figures 2 and SI1, Supporting Information). Such structural characteristics can influence some of the electronic and physical properties of the material.[34] In the HOMO of **9a,b**, $\pi$ electrons are able to delocalize over the whole bis[5-(fluoren-2-yl)thiophen-2-yl]benzothiadiazole core and end-capped carbazole dendrons through the lone electron pair of the nitrogen of the carbazole, whereas in the HOMO of **9c**, $\pi$ electrons delocalize over the bis(carbazol-$N'$-yl)carbazole moiety of the dendron. In the LUMO of **9a–c**, the excited electrons localized on the electron-deficient benzothiadiazole core, creating donor–acceptor characteristics.

**Photophysical Properties.** The optical properties of the dendrimers **9a–c** were investigated in $CH_2Cl_2$ solutions and thin films spin coated on quart substrates. The pertinent data are summarized in Table 1. In view of the electronic absorption spectra obtained in $CH_2Cl_2$, all dendrimers show very similar spectral features, which are basically composed of three major absorption bands: characteristic absorption bands ascribed to the $\pi$–$\pi^*$ electron transition of the carbazole and fluoren-2-yl)thiophene moieties at ∼298 and ∼371 nm, respectively, with the band at the longer wavelength (∼514 nm) belonging to a donor (the end-capped carbazole dendrons) to acceptor (2,1,3-benzothiadiazole core) intramolecular charge-transfer (ICT) transition (Figure 3). Upon photoexcitation, all three

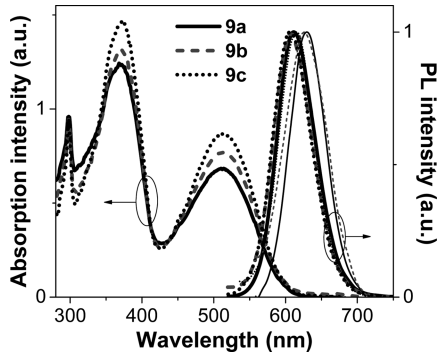


**Figure 3.** Absorption and PL spectra of **9a–c** measured in $CH_2Cl_2$ (thick line) and thin films (thin line) spin coated on quartz substrates.

compounds transmit red fluorescence in dilute solutions. Their solution photoluminescence (PL) spectra exhibit featureless emission bands, with the emission peaks centered around 606–611 nm. The emission peaks are blue shifted with the increasing generation of the end-capped dendrons, indicating that the donor–acceptor feature in the molecules is getting weaker and weaker, supporting by the TDDFT-based calculation results. The PL spectra of **9a–c** are excitation-wavelength independent, where, because of excitation at either carbazole moieties (at 298 nm) or bis[5-(fluoren-2-yl)-thiophen-2-yl]benzothiadiazole core (at 371 and 514 nm), the emission spectra obtained are identical. This indicates that energy or excitons can efficiently be transferred from the carbazole moiety to the emissive core. These materials show Stokes shifts in the range of 92–98 nm, suggesting less energy loss during the relaxation process and efficient fluorescence. The solution fluorescence quantum yields ($\Phi_F$) of **9a–c** measured in $CH_2Cl_2$ using coumarin 6 as a standard are in the range of 0.10–0.39 (Table 1). The photoinduced ICT process in these materials accounts for their low $\Phi_F$ resulting from the fluorescence quenching by electron exchange according to the Dexter mechanism.[35] The decrease in quantum yield resulting from the photoinduced ICT process is a common phenomenon for organic compounds.[36,37] However, these dendrimers show good fluorescence in the solid state. Their thin-film PL spectra also show featureless emission bands and they exhibit small red shifts (∼10–19 nm) in their emission maxima as compared to those obtained from $CH_2Cl_2$ (Figure 3). This suggests that the


dx.doi.org/10.1021/am402349v | ACS Appl. Mater. Interfaces 2013, 5, 8694–8703

intermolecular $\pi-\pi$ interactions in the solid state of the fluorescent core are prevented by the bulky molecular structure of the rigid carbazole dendrons.

**Electrochemical and Thermal Properties.** To analyze the redox properties of dendrimers **9a–c**, cyclic voltammetry (CV) measurements performed in a three-electrode cell set up with 0.1 M $Bu_4NPF_6$ as a supporting electrolyte in $CH_2Cl_2$ under an inert atmosphere were carried out. The results are depicted in Figure 4a and tabulated in Table 1. CV curves of all

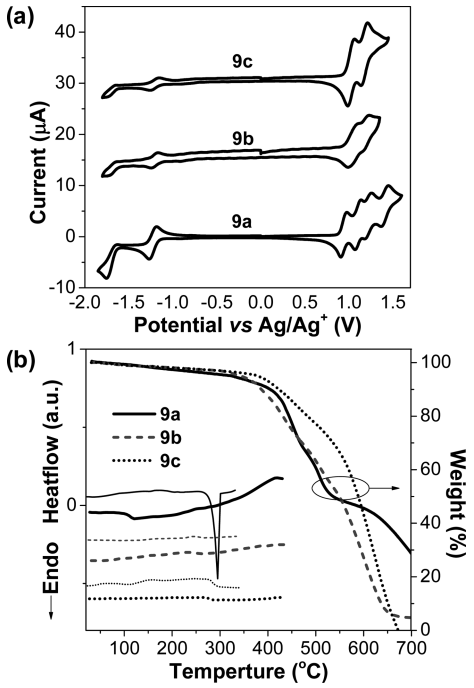


**Figure 4.** (a) CV traces measured at a scan rate of 50 mV $s^{-1}$ and (b) DSC (1st heating scan (thick line), 2nd heating scan (thin line)) and TGA thermograms of **9a–c** measured at a heating rate of 10 °C $min^{-1}$ of **9a–c**.

compounds exhibit well-defined two quasi-reversible reduction waves at $E_{1/2}$ of ∼−1.15– −1.22, and −1.69 V, which correspond to the formation of the anion radical of the electron-poor 2,1,3-benzothiadiazole moiety.[38,39] The CV curve of **9a** displays four well-separated quasi-reversible oxidation waves, whereas the CV traces of both **9b** and **9c** show two oxidation processes. The first oxidation wave is assigned to the removal of electrons from the peripheral carbazoles, resulting in radical cations. It is noted that the potential ($E_{1/2}$) of the first oxidation wave of **9a** (0.94 V) appears at a lower potential than those of **9b** (1.04), **9c** (1.02 V), and *N*-alkylcarbazole ($E^{ox}_{1/2}$ = 1.09 V), indicating $\pi$-electron conjugation between the carbazole and core unit, as observed in the quantum calculation results. Importantly, multiple CV scans of all compounds reveal identical CV curves with no additional peak at a lower potential on the cathodic scan ($E_{pc}$) being observed, suggesting no electrochemical coupling at the 3,6-positions of the carbazole peripheries because they are protected by *tert*-butyl groups. All newly synthesized dendrimers are electrochemically stable molecules, as expected. The HOMO and LUMO energy levels of **9a–c** are calculated from their oxidation onset potentials ($E^{ox}_{onset}$) and energy gaps ($E_g$), and the results are listed in Table 1. The HOMO energy levels of **9a–c** are in the range of −5.33 to −5.40 eV, which match quite well with the work function of commonly used hole-injection/transport layers and anodes such as PEDOT/PSS (−5.00 eV) and ITO (−4.80 eV), indicating that these materials are suitable for applications in OLEDs as hole-transporting red emitters. Their LUMO levels calculated by subtracting the energy band gaps ($E_g^{opt}$) from the HOMO levels range from −3.25 eV for **9a**, −3.31 eV for **9b**, and −3.33 eV for **9c**, which are close to the work function of the LiF/Al anode (−4.20 eV) and seem suitable for efficient electron injection. The energy gaps ($E_g^{ele}$) of these dendrimers calculated from the oxidation and reduction onset potentials are in the range of 2.05–2.09 eV, which are nearly identical to those estimated from their corresponding UV–Vis absorption spectra ($E_g^{opt}$ = 2.07–2.08 eV), indicating that the electrochemical measurement of the LUMO and HOMO energy levels is reliable (Table 1).

The thermal properties of dendrimers **9a–c** were analyzed by differential scanning calorimetry (DSC) and thermogravimetric analysis (TGA), and the results are shown in Figure 4b and Table 1. DSC measurement of an as-prepared sample of **9a** reveals an endothermic peak because of the melting point at 295 °C in the first heating scan, whereas in the second heating scan, the DSC thermogram shows an endothermic baseline shift owing to the glass transition ($T_g$) at 115 °C with no crystallization and melting detected at higher temperatures. The first- and second-scan DSC traces of as-prepared samples of **9b** and **9c** having a higher generation of the carbazole dendrons as the end-caps exhibit only an endothermic baseline shift at the $T_g$ values of 256 and 283 °C, respectively, indicating the high thermal stability of the amorphous materials. The thermal stabilities of these dendrimers were further confirmed by TGA measurements that showed an increasing 5% weight-loss temperature ($T_{5d}$) from 326 °C for **9a**, 344 for **9b**, and 378 °C for **9c**. It is noted that as the size of the dendrons increased the thermal and phase-transition properties ($T_g$ and $T_{5d}$) of these dendrimers improved. This may be due to a rigid and bulky structure of the carbazole dendron. These results suggest that the presence of carbazole dendrons as end-caps in the molecule not only improve its thermal stability but also reduce the crystallization of a planar-conjugated core and induce the formation of an amorphous form, which in turn could increase the service time in device operation and enhance the morphological stability of the thin film. Moreover, the ability to form a molecular glass with the possibility of preparing good thin films by both evaporation and solution-casting processes is highly desirable for applications in electroluminescent devices.

**Electroluminescent Properties.** According to the above-discussed excellent properties, including suitable HOMO–LUMO energy levels, good luminescence properties, high thermal stability, good amorphous morphological stability, and the ability to form good thin films from a solution spin-coating process, dendrimers **9a–c** show great potential for use as solution-processed nondoped hole-transporting red emitters in OLEDs. The OLED devices (I–V) using **9a–c** as an emitting layer (EML) were fabricated. The **9a–c** layers were spin coated from a $CHCl_3$/toluene (1:1) solution with controlled thickness. The electroluminescent (EL) spectra and characteristics of the devices are illustrated in Figures 5 and 6 (also, see the Supporting Information), and all parameters are summarized in Table 2. First, simple single-layer OLEDs using **9c** as an EML with the device structure of ITO/**9c** (spin coating)(30–40 nm)/LiF(0.5 nm)–Al(150 nm) (device I) and ITO/PEDOT–PSS/**9c** (spin coating)(30–40 nm)/LiF(0.5 nm)–Al(150 nm) (device II) were fabricated and characterized. As the devices

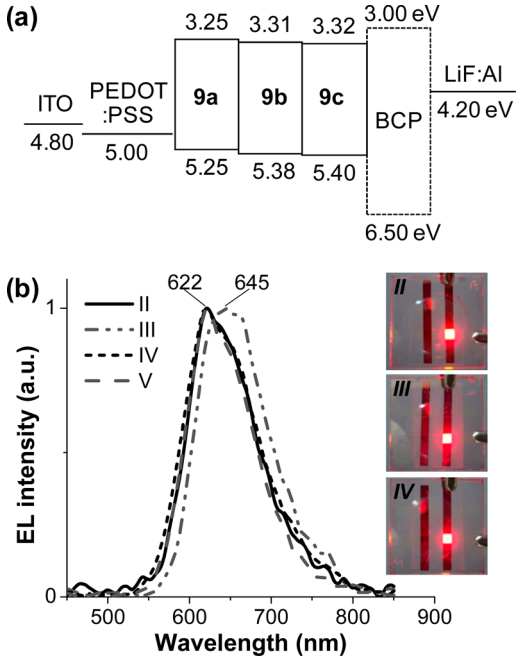


**Figure 5.** (a) Schematic energy diagram and (b) EL spectra of the **9a–c**-based OLEDs (devices II–V).

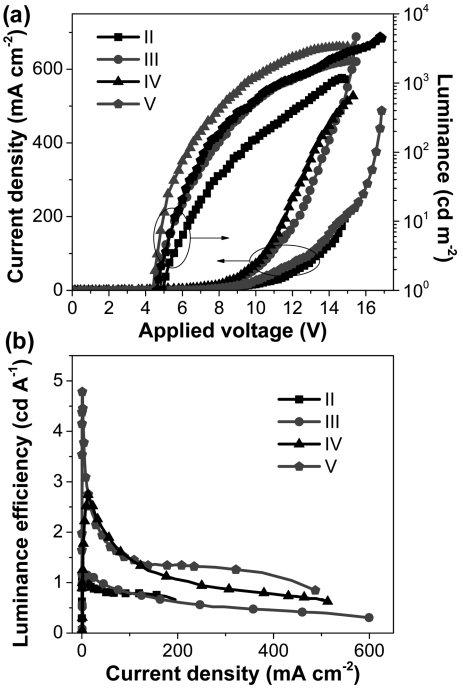


**Figure 6.** Plots of (a) current density–voltage–luminance ($I$–$V$–$L$) and (b) efficiency–current density ($\eta$–$I$) characteristics of the OLEDs (devices II–V).

were fabricated identically, the differences between them should indicate the improvement achieved with the new material or device structure. From this study and other reports,[40,41] it was found that the incorporation of a conductive polymer, poly(3,4-ethylenedioxythiophene)/poly(4-styrenesulfonate) (PEDOT/PSS), in the device as a hole-injection layer not only increased the maximum luminance efficiency ($\eta_{max}$) of the OLED from 0.46 cd $A^{-1}$ at 10.0 mA $cm^{-2}$ (device I) to 1.15 cd $A^{-1}$ at 1.5 mA $cm^{-2}$ (device II) but also significantly decreased the turn-on voltage ($V_{on}$) of the OLED from 6.0 V (device I) to 4.9 V (device II). It has been pointed out that the lower operating voltage of the PEDOT/PSS-based device can be attributed to the rough and porous surface of the spin-coated PEDOT/PSS polymer layer, which increases the contact area to enhance hole injection and lowers the barrier at the organic–organic interface by relocating the barrier to the more conductive PEDOT/PSS layer.[42] Under the applied voltage, both devices emit a bright-red luminescence with good color purity, emission peaks around 622–624 nm, and full-width at half-maxima (fwhm) of ~95 nm. The Commission Internationale De L'Eclairage (CIE) coordinates of the emitted light are $x$ = 0.63 and $y$ = 0.35, which are close to the National Television System Committee (NTSC) standard red (0.67, 0.33) as the pure red color.[43] The EL spectra of the diodes are nearly identical and match with the PL spectrum of **9c**. The **9c**-based red OLED (device II) shows a maximum brightness ($L_{max}$) of 1135 cd $m^{-2}$ at 14.8 V, $\eta_{max}$ of 1.15 cd $A^{-1}$ at 1.5 mA $cm^{-2}$, and a $V_{on}$ of 4.9 V. The high-EL efficiency of the **9c**-based device despite its low PL quantum yield might come from a combination of the ICT effect and a good balance of its HOMO and LUMO energy levels.

The efficiency of the single-layer OLED could be further improved by balancing the charge injection in the device. It has been known that the effective recombination of electrons and holes affects the electroluminescence efficiency of OLEDs.[44] Analysis of the band-energy diagram of device II reveals that a barrier for electron injection at the EML/LiF–Al interface (~0.88 eV) is about twofold higher than that for hole migration at the PEDOT–PSS/EML interface (~0.40 eV) (Figure 5a), indicating that **9c** is the more hole-injection EML. To balance the charge injection in this device, therefore, an electron-injection/hole-blocking layer in between the interface of the EML and LiF layers is required. Dimethyl-4,7-diphenyl-1,10-phenanthroline (BCP) is known to enhance the performance of multilayer devices fabricated with a predominantly hole-transporting emitter.[45] Therefore, to enable the higher performance of the devices, PEDOT/PSS as a hole-injection layer and BCP as a hole-blocking layer (HBL) were incorporated between the ITO electrode and EML layer, and between the EML layer and LiF–Al electrode, respectively. Simple double-layer OLEDs (devices III–V) using **9a–c** as an EML with the device structure of ITO/PEDOT–PSS/**9a–c** (spin coating)(30 nm)/BCP(40 nm)/LiF(0.5 nm)/Al(150 nm) were fabricated. The EL spectra and current density–voltage–luminance ($I$–$V$–$L$) characteristics of the devices are shown in Figures 5 and 6 and the data are listed in Table 2. The **9c**-based spin-coating double-layer device (V) exhibits a high $L_{max}$ value of 4655 cd $m^{-2}$ at 16.6 V and a $\eta_{max}$ value of 4.80 cd $A^{-1}$ at 1.2 mA $cm^{-2}$, which corresponds to a 76% improvement compared to that of the standard device (II) without BCP ($\eta_{max}$ = 1.15 cd $A^{-1}$). The EL spectrum of device V exhibit a featureless emission peak identical to the thin-film PL spectrum of **9c** and also its single-layer device (II), indicating that they have similar relaxation processes. These results proved that the insertion of a BCP layer between the two layers helps to block holes flowing to the cathode and accumulate the hole at the EML and HBL interface, resulting in an increasing probability for electrons and holes to combine at the EML layer. The luminance characteristics and emission efficiency of the device are improved while maintaining a good red-emission quality. The **9c**-based red OLED (device V) is the best performing device among all of these analogues. The device exhibits a high


dx.doi.org/10.1021/am402349v | ACS Appl. Mater. Interfaces 2013, 5, 8694–8703

**Table 2. Electroluminescent Data of OLEDs Based on Dendrimers 9a−c**

| device | EML | $\lambda_{max}^{EL}$ (fwhm) (nm) | $V_{on}/V_{100}$ (V)[d] | $L_{max}$ (cd m$^{-2}$) (at the voltage (V))[e] | $J_{max}$ (mA cm$^{-2}$)[f] | $\eta_{max}$ (cd A$^{-1}$) (at mA cm$^{-2}$)[g] | CIE ($x$, $y$) |
|---|---|---|---|---|---|---|---|
| I[a] | **9c** | 624 (99) | 6.0/9.8 | 1109 (13.4) | 616 | 0.46 (10.0) | 0.63, 0.35 |
| II[b] | **9c** | 622 (93) | 4.9/9.3 | 1135 (14.8) | 194 | 1.15 (1.5) | 0.63, 0.35 |
| III[c] | **9a** | 645 (101) | 4.4/7.6 | 2106 (15.2) | 599 | 1.16 (14.6) | 0.65, 0.33 |
| IV[c] | **9b** | 622 (101) | 4.4/6.4 | 3354 (15.0) | 513 | 2.75 (15.4) | 0.63, 0.36 |
| V[c] | **9c** | 622 (93) | 4.5/7.2 | 4655 (16.6) | 439 | 4.80 (1.2) | 0.63, 0.35 |

[a]ITO/EML(spin coating)/LiF−Al. [b]ITO/PEDOT−PSS/EML(spin coating)/LiF−Al. [c]ITO/PEDOT−PSS/EML(spin coating)/BCP/LiF−Al. [d]Voltages at luminance values of 1 and 100 cd m$^{-2}$. [e]Maximum luminance at the applied voltage. [f]Current density at maximum luminance. [g]Luminance efficiency.

$\eta_{max}$ value of 4.80 cd A$^{-1}$ at 1.2 mA cm$^{-2}$ and a $V_{on}$ value of 4.5 V, whereas the **9b**-based device (IV) shows lower EL properties with an $L_{max}$ value of 3345 cd m$^{-2}$ at 15.0 V, an $\eta_{max}$ value of 2.75 cd A$^{-1}$ at 15.4 mA cm$^{-2}$, and a $V_{on}$ value of 4.4 V. The **9a**-base device (III) shows the lowest device performance, with an $\eta_{max}$ value of 1.16 cd A$^{-1}$ at 14.6 mA cm$^{-2}$. The significantly higher light-emission efficiencies in devices IV and V compared to that of the device III could be explained by a combination of the suitable HOMO (−5.38 to −5.40) and LUMO (−3.31 to −3.32) levels for efficient charge injection and the high-quality spin-coated films of the EMLs (**9b** and **9c**). Under the applied voltages, all OLEDs emit a bright-red emission with featureless patterns, emission peaks around 622−645 nm, and fwhm of ∼93−101 nm (Figure 5b and Table 2). In particular, the **9a**-based red OLED (device III) emits red light with high color purity at about 645 nm and CIE coordinates of (0.65, 0.33), which are very close to the NTSC standard red (0.67, 0.33). The EL spectra of devices III−V are identical to their thin-film PL spectra, indicating that the EL purely originates from their corresponding dendrimers. Furthermore, no emission shoulder at a longer wavelength resulting from the excimer and exciplex species formed at the interface of the EML and BCP layers, which often occurs in devices fabricated from EMLs with planar molecular structure,[46] is detected. Moreover, stable emission is obtained from all devices, and the EL spectra did not change over the entire driven voltages (Figure SI2, Supporting Information). As far as we know, the ability of **9c** as a solution-processable nondoped red EML in red OLEDs, in terms of device performance, thermal property, red color purity, and simple device structure, is outstanding compared with those of other solution-processable red fluorescent emitters[13−26] and our recently reported solution-processable red fluorescent emitters[27] and is comparable with vacuum-deposited red fluorescent emitters reported in recent years.[8,47] These preliminary results imply that **9c** serves as an attractive candidate for light-emitting materials that can be used in solution-processed nondoped red OLEDs with high luminance efficiency and excellent color purity, although further studies are necessary for practical applications.

## CONCLUSIONS

We demonstrated the design strategy and synthesis of bis[5-(fluoren-2-yl)thiophen-2-yl]benzothiadiazole-cored carbazole dendrimers (**9a−c**) as a nondoped solution-processed red-light emitters for OLEDs. By using carbazole dendrons as the end caps, we are able to reduce the crystallization and retain the high emissive ability of a planar red fluorescent core in the solid state as well as improve the amorphous stability of the material. These dendrimers can form morphologically stable amorphous thin films with $T_g$ as high as 283 °C. They exhibit a bright-red fluorescence with a hole-transporting property. A **9c**-based single-layer red OLED with a maximum luminance efficiency as high as 1.15 cd A$^{-1}$ is achieved. Simple structured solution-processed OLEDs using these dendrimers as hole-transporting nondoped emitters and BCP as a hole-blocking layer emits a stable red color around 622−645 nm with high luminance efficiencies (up to 4.80 cd A$^{-1}$ at 1.2 mA cm$^{-2}$) and CIE coordinates of (0.65, 0.33), which is close to the pure red color. This report offers a useful strategy to decorate the highly efficient but planar fluorophore so that it is suitable for applications in solution-processed OLEDs and to prepare high $T_g$ amorphous materials for high-temperature applications.

## ASSOCIATED CONTENT

### Supporting Information

Optimized structure of the compounds calculated by B3LYP/6-31G(d) in the gas phase; calculated HOMO, LUMO, and HOMO−LUMO energy gap of the studied compounds by B3LYP/6-31G(d) in the gas phase; normalized EL spectra of the double layer OLEDs at different applied voltages; and $^1$H to $^{13}$C NMR spectra of compounds **2−8** and **9a−c**. This material is available free of charge via the Internet at http://pubs.acs.org.

## AUTHOR INFORMATION

### Corresponding Author

*Fax: +66 44 224648. E-mail: pvinich@sut.ac.th.

### Notes

The authors declare no competing financial interest.

## ACKNOWLEDGMENTS

This work was financially supported by the Thailand Research Fund (DBG 5580001). We acknowledge scholarship support from the Center of Excellence for Innovation in Chemistry (PERCH−CIC) and the Science Achievement Scholarship of Thailand (SAST).

## REFERENCES

(1) Tang, C. W.; Van Slyke, S. A. *Appl. Phys. Lett.* **1987**, *51*, 913−915.
(2) So, F.; Kido, J.; Burrows, P. L. *MRS Bull.* **2008**, *33*, 663−669.
(3) Zhu, X.-H.; Peng, J.; Cao, Y.; Roncali, J. *Chem. Soc. Rev.* **2011**, *40*, 3509−3524.
(4) Perepichka, D. F.; Perepichka, I. F.; Meng, H.; Wudl, F.; Meng, H.; Herron, N. In *Organic Light-Emitting Materials and Devices*, 1st ed.; Li, Z., Meng, H., Eds.; Taylor & Francis Group: Boca Raton, FL, 2007; p 45.
(5) Lo, S. C.; Burn, P. L. *Chem. Rev.* **2007**, *107*, 1097−1116.
(6) Bernhardt, S.; Kastler, M.; Enkelmann, V.; Baumgarten, M.; Müllen, K. *Chem.—Eur. J.* **2006**, *12*, 6117−6128.
(7) Kwok, C. C.; Wong, M. S. *Macromolecules* **2001**, *34*, 6821−6830.
(8) Chen, C. *Chem. Mater.* **2004**, *16*, 4389−4400.
(9) Zhang, X. H.; Chen, B. J.; Lin, X. Q.; Wong, O. Y.; Lee, C. S.; Kwong, H. L.; Lee, S. T.; Wu, S. K. *Chem. Mater.* **2001**, *13*, 1565−1569.

(10) Zhu, M.; Li, Y.; Hu, S.; Li, C.; Yang, C.; Wu, H.; Qin, J.; Cao, Y. *Chem. Commun.* **2012**, *48*, 2695−2697.
(11) Huang, J.; Qiao, X.-F.; Xia, Y.-J.; Zhu, X.-H.; Ma, D.-G.; Cao, Y.; Roncali, J. *Adv. Mater.* **2008**, *20*, 4172−4175.
(12) Huang, J.; Liu, Q.; Zou, J.-H.; Zhu, X.-H.; Li, A.-Y.; Li, J.-W.; Wu, S.; Peng, J. B.; Cao, Y.; Xia, R.; Bradley, D. D. C.; Roncali, J. *Adv. Funct. Mater.* **2009**, *19*, 2978−2986.
(13) Zhou, Y.; He, Q. G.; Yang, Y.; Zhong, H. Z.; He, C.; Sang, G. Y.; Liu, W.; Yang, C. H.; Bai, F. L.; Li, Y. F. *Adv. Funct. Mater.* **2008**, *18*, 3299−3306.
(14) Takada, K.; Ichimura, M.; Ishibashi, T.; Tamura, S. *Jpn. Kokai Tokkyo Koho* JP2001131128, 2001; p 44.
(15) Yeh, H.-C.; Yeh, S.-J.; Chen, C.-T. *Chem. Commun.* **2003**, 2632−2633.
(16) Shimizu, M.; Kaki, R.; Takeda, Y.; Hiyama, T.; Nagai, N.; Yamagishi, H.; Furutani, H. *Angew. Chem., Int. Ed.* **2012**, *51*, 4095−4099.
(17) Li, J.; Li, Q.; Liu, D. *ACS Appl. Mater. Interfaces* **2011**, *3*, 2099−2107.
(18) Li, Q.; Li, J.; Yang, R.; Deng, L.; Gao, Z.; Liu, D. *Dyes Pigm.* **2011**, *92*, 674−680.
(19) Wang, J.-L.; Zhou, Y.; Li, Y.; Pei, J. *J. Org. Chem.* **2009**, *74*, 7449−7456.
(20) Wang, Z.; Lu, P.; Xue, S.; Gu, C.; Lv, Y.; Zhu, Q.; Wang, H.; Ma, Y. *Dyes Pigm.* **2011**, *91*, 356−363.
(21) Gao, B.; Zhou, Q.; Geng, Y.; Cheng, Y.; Ma, D.; Xie, Z.; Wang, L.; Wang, F. *Mater. Chem. Phys.* **2006**, *99*, 247−252.
(22) Sun, X.; Xu, X.; Qiu, W.; Yu, G.; Zhang, H.; Gao, X.; Chen, S.; Song, Y.; Liu, Y. *J. Mater. Chem.* **2008**, *18*, 2709−2715.
(23) Zhao, Z.; Geng, J.; Chang, Z.; Chen, S.; Deng, C.; Jiang, T.; Qin, W.; Lam, J. W. Y.; Kwok, H. S.; Qiu, H.; Liu, B.; Tang, B. Z. *J. Mater. Chem.* **2012**, *22*, 11018−11021.
(24) Yeh, H.-C.; Chan, L.-H.; Wua, W.-C.; Chen, C.-T. *J. Mater. Chem.* **2004**, *14*, 1293−1298.
(25) Lee, Y.-T.; Chiang, C.-L.; Chen, C.-T. *Chem. Commun.* **2008**, 217−219.
(26) Li, D.; Wang, K.; Huang, S.; Qu, S.; Liu, X.; Zhu, Q.; Zhang, H.; Wang, Y. *J. Mater. Chem.* **2011**, *21*, 15298−15304.
(27) Khanasa, T.; Prachumrak, N.; Rattanawan, R.; Jungsuttiwong, S.; Kaewin, T.; Sudyoadsuk, T.; Tuntulani, T.; Promarak, V. *Chem. Commun.* **2013**, *49*, 3401−3403.
(28) Moonsin, P.; Prachumrak, N.; Rattanawan, R.; Keawin, T.; Jungsuttiwong, S.; Sudyoadsuk, T.; Promarak, V. *Chem. Commun.* **2012**, *48*, 3382−3384.
(29) Kartens, T.; Kobs, K. *J. Phys. Chem.* **1980**, *84*, 1871−1872.
(30) Lee, S. H.; Tsutsui, T. *Thin Solid Films* **2000**, *363*, 76−80.
(31) Frisch, M. J.; Trucks, G. W.; Schlegel, H. B.; Scuseria, G. E.; Robb, M. A.; Cheeseman, J. R.; Scalmani, G.; Barone, V.; Mennucci, B.; Petersson, G. A.; Nakatsuji, H.; Caricato, M.; Li, X.; Hratchian, H. P.; Izmaylov, A. F.; Bloino, J.; Zheng, G.; Sonnenberg, J. L.; Hada, M.; Ehara, M.; Toyota, K.; Fukuda, R.; Hasegawa, J.; Ishida, M.; Nakajima, T.; Honda, Y.; Kitao, O.; Nakai, H.; Vreven, T.; Montgomery, Jr., J. A.; Peralta, J. E.; Ogliaro, F.; Bearpark, M.; Heyd, J. J.; Brothers, E.; Kudin, K. N.; Staroverov, V. N.; Kobayashi, R.; Normand, J.; Raghavachari, K.; Rendell, A.; Burant, J. C.; Iyengar, S. S.; Tomasi, J.; Cossi, M.; Rega, N.; Millam, J. M.; Klene, M.; Knox, J. E.; Cross, J. B.; Bakken, V.; Adamo, C.; Jaramillo, J.; Gomperts, R.; Stratmann, R. E.; Yazyev, O.; Austin, A. J.; Cammi, R.; Pomelli, C.; Ochterski, J. W.; Martin, R. L.; Morokuma, K.; Zakrzewski, V. G.; Voth, G. A.; Salvador, P.; Dannenberg, J. J.; Dapprich, S.; Daniels, A. D.; Farkas, Ö.; Foresman, J. B.; Ortiz, J. V.; Cioslowski, J.; Fox, D. J. *Gaussian 09*, revision A.1; Gaussian, Inc.: Wallingford, CT, 2009.
(32) Forrest, S. R.; Bradley, D. D. C.; Thomson, M. E. *Adv. Mater.* **2003**, *15*, 1043−1048.
(33) Li, Y.; Li, A.-Y.; Li, B.-X.; Huang, J.; Zhao, L.; Wang, B.-Z.; Li, J.-W.; Zhu, X.-H.; Peng, J.; Cao, Y.; Ma, D.-G.; Roncali, J. *Org. Lett.* **2009**, *11*, 5318−5321.
(34) Ning, Z. J.; Zhou, Y. C.; Zhang, Q.; Ma, D. G.; Zhang, J. J.; Tian, H. *J. Photochem. Photobiol. A* **2007**, *192*, 8−16.
(35) Collado, D.; Casado, J.; González, S. R.; Navarrete, J. T. L.; Suau, R.; Perez-Inestrosa, E.; Pappenfus, T. M.; Raposo, M. M. M. *Chem.—Eur. J.* **2011**, *17*, 498−507.
(36) Qu, J. Q.; Pschirer, N. G.; Liu, D. J.; Stefan, A.; Schryver, F. C. D.; Müllen, K. *Chem.—Eur. J.* **2004**, *10*, 528−537.
(37) Ohkita, H.; Benten, H.; Anada, A.; Noguchi, H.; Kido, N.; Ito, S.; Yamamoto, M. *Phys. Chem. Chem. Phys.* **2004**, *6*, 3977−3984.
(38) Shen, M.; Rodríguez-López, J.; Huang, J.; Liu, Q.; Zhu, X.-H.; Bard, A. J. *J. Am. Chem. Soc.* **2010**, *132*, 13453−13461.
(39) Watanabe, M.; Goto, K.; Fujitsuka, M.; Tojo, S.; Majima, T.; Shinmyozu, T. *Bull. Chem. Soc. Jpn.* **2010**, *83*, 1155−1161.
(40) Kirchmeyer, S.; Reuter, K. *J. Mater. Chem.* **2005**, *15*, 2077−2088.
(41) Mu, H.; Li, W.; Jones, R.; Steckl, A.; Klotzkin, D. *J. Lumin.* **2007**, *126*, 225−229.
(42) Kim, W.; Kushto, G.; Kim, G.; Kafafi, Z. *J. Polym. Sci., Part B* **2003**, *41*, 2522−2528.
(43) Kuo, T.-W.; Chung, H.-P.; Chen, T.-M. *Chem. Lett.* **2010**, *39*, 200−201.
(44) Zhang, S. T.; Wang, Z. J.; Zhao, J. M.; Zhan, Y. Q.; Wu, Y.; Zhou, Y. C.; Ding, X. M.; Hou, X. Y. *Appl. Phys. Lett.* **2004**, *84*, 2916−2918.
(45) Tang, C.; Liu, F.; Xia, Y.-J.; Lin, J.; Xie, L.-H.; Zhong, G.-Y.; Fan, Q.-L.; Huang, W. *Org. Electron.* **2006**, *7*, 155−162.
(46) Kim, D. Y.; Cho, H. N.; Kim, C. Y. *Prog. Polym. Sci.* **2000**, *25*, 1089−1139.
(47) Thomas, K. R. J.; Lin, J. T.; Velusamy, M.; Tao, Y.-T.; Chuen, C.-H. *Adv. Funct. Mater.* **2004**, *14*, 83−90.